

Geometry Calibration of a Dual Headed SPECT System, with Rocking Motion Correction, for Small Animal Imaging

V-H Tran¹, M.F. Smith¹, S.R. Meikle², B.L. Welch¹, J.S. Goddard³, J.S. Baba², A.G. Weisenberger¹

Abstract– A method for simultaneous geometry calibration of a dual detector SPECT system for small animal imaging is presented. For multi-headed SPECT systems, it is desirable that all detectors are calibrated with respect to a common spatial coordinate system, so that projection data from both detectors can be used to reconstruct the common object in the same image space. We adapted Bequé’s geometry calibration procedure. We show that the procedure can be applied to a dual-headed imaging system by optimizing the combined objective function. Initially, the measured and predicted paths of calibration point sources had significant systematic difference which was dominant in the axial direction. The problem was caused by flexing of the gantry support due to the heavy weight of the detectors. While various correction models of different complexity and assumptions could be applied, we found that the errors were corrected well by including an angle-dependent sinusoidal function to the z-coordinate.

I. INTRODUCTION

The SPECT imaging system has two gamma-ray detectors (Fig. 1) and an optical tracking system designed to image awake mice [1]-[2]. The gamma-ray detectors have a 10 cm x 20 cm field of view and are constructed using 2 mm x 2 mm x 15 mm pixellated NaI(Tl) scintillators, with 0.25 mm inter-crystal spacing. To optimize imaging options, one detector is fitted with a parallel hole collimator, while the other, a pinhole collimator. The detector fitted with the parallel hole collimator can image the whole mouse, while the detector with the pinhole collimator can focus in on a region of interest, e.g. the brain (Fig. 2). For a pinhole camera, a model of projection geometry can be characterized by seven parameters [3], while for the detector with a parallel hole collimator, the geometry can be characterized by a smaller set of five parameters, without the distances from the pinhole to axis of rotation and to the detector. The parameter values for a particular geometry can be accurately determined by non-linear least squares iterative fitting. For geometry calibration, we used 360° of

projection data of a calibration phantom composed of three point sources arranged in a triangular figuration [4].

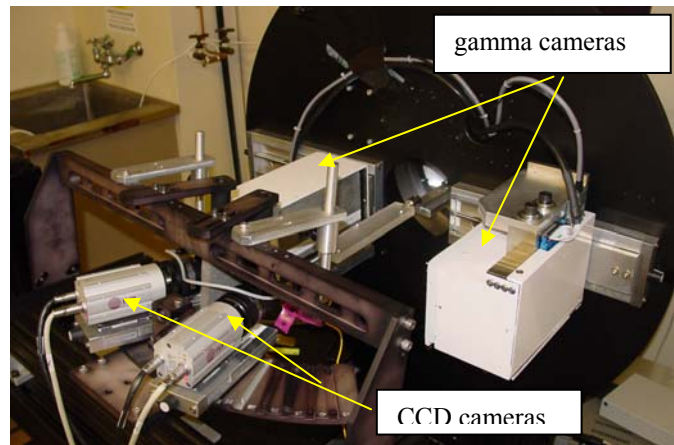


Fig. 1 A SPECT imaging system with two gamma-ray detectors and an optical tracking system consisting of 2 CCD cameras.

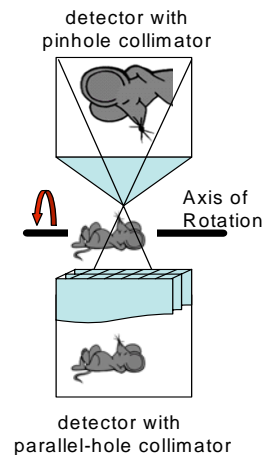


Fig. 2. A dual-headed SPECT system with one detector fitted with a pinhole collimator and the other a parallel-hole collimator.

In this work, we introduce two additional parameters (amplitude of axial oscillation and its phase angle) for each detector to model the observed axial excursion due to flexing of the detector gantry, plus a third parameter for the phase angle between the pinhole and parallel hole detectors. The

Manuscript submitted on October 1st, 2005.

Support for this research is from the Department of Energy (DOE) Office of Biological and Environmental Research in the Office of Science through DOE Medical Imaging Program and from the DOE Office of Nuclear Physics

V. H. Tran (e-mail: timtran@jlab.org), M. F. Smith, B. L. Welch, A. G. Weisenberger are with Thomas Jefferson National Accelerator Facility, Newport News, VA 23606, USA.

S. R. Meikle (smeikle@fhs.usyd.edu.au), is with the school of Medical Radiation Sciences, University of Sydney, Australia.

J. S. Baba (babajs@ornl.gov), J. S. Goddard, Oak Ridge National Laboratory, Oak Ridge, TN, USA.

projection data from both detectors could then be used to reconstruct the common object in the same image space.

II. PROJECTION ERROR RESULTING FROM GANTRY FLEXING

Undesirable detector motion can arise from a combination of gantry flexing and even possibly axial travel in the bearing support. This causes a definite angle-dependent movement of the detector with respect to the axis of rotation (AOR). The effect is observable by a predictable angle-dependent movement in the projected image of calibration point sources. In our case, the movement is predominantly in the axial direction. From projections obtained over 360 degrees of rotation, Fig.3 shows the differences in the measured and predicted distances in the axial direction for three calibration point sources in a phantom (Fig. 7). An axial movement of 1 mm by the detector due to flexing or travel in the bearing could have resulted in a 3 mm movement in measured projections when magnification factor of 3 was used. Fig. 4 shows a good agreement between measurements and predictions in the radial direction. Effort was focused on deriving a semi-empirical correction model to account for the observed deviance. Flexing and travel can occur in several ways depending on the strength and location of detector support to the gantry. As a result, an appropriate correction function may be specific to a gantry design. Fig. 5 shows how an undesirable gantry motion can manifests itself as a small turning motion when a heavy detector is supported by a metal bracket on one side of the detector. The metal bracket is mounted on a motorized sliding stage such that the distance between the detector and the mouse can be adjusted for different projection magnification factor (Fig. 5A). In an ideal case, when the gantry support is totally rigid, the detector maintains the same orientation with the axis of rotation during its 360 degrees of rotation (Fig. 5B). The normal ray, which is incident normally on the detector after coming through the pinhole, should maintain its axial position for all angular positions. However, due to flexing, there is usually a small bending movement due to the weight of the detector (Fig. 5C). When the detectors rotate 360 degrees during data acquisition, the normal ray will oscillate about a mean axial position z^0 . Maximum deviation usually occurs when the detector is at the top and bottom position.

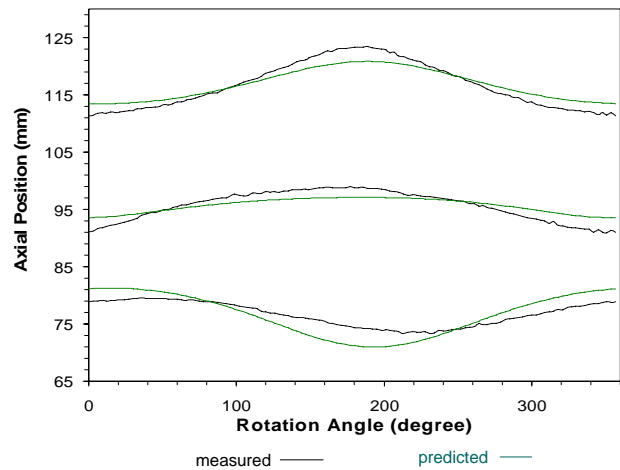


Fig. 3. Graphs showing differences in the measured and predicted distances in the axial direction for the three point sources used in calibration.

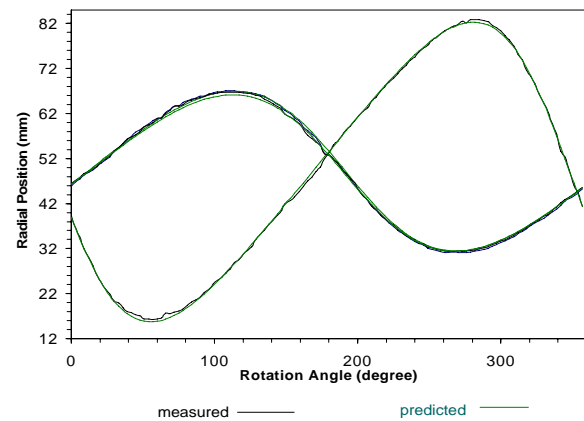


Fig.4. Graphs showing good agreement in the measured and predicted distances in the radial direction for the three point sources used in calibration. Overlapping is due to two of the three co-planar point sources have the same radial distance.

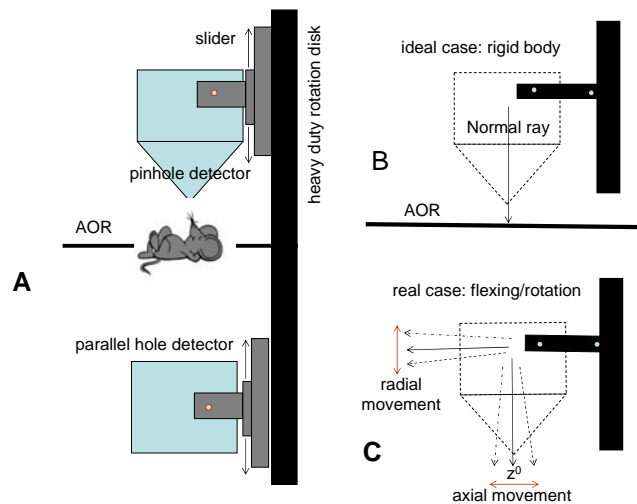


Fig. 5. (A) Cartoon showing the detector mounted on a sliding stage. (B) The normal ray through the pinhole maintains its normality with the AOR at all position in an ideal rigid gantry. (C) The normal ray has a small sweep motion caused by the flexing of a non-rigid gantry.

III. AN APPROXIMATE PROJECTION MODEL INCORPORATING AXIAL MOTION

A simple model to explain the observed axial movement is to assume the detector is rocking with a small angle about a pivot point. The exact location of a pivot point in the flexing support arm is not apparent. An assumption about the location is made based on empirical data. If the pivot point is at the sliding stage, then the magnitude of radial movement of the detector would be proportional to the perpendicular distance between the pivot point and the normal ray (Fig. 5C). However, a significant radial movement of the detector during a 360 revolution was not evident. If the pivot point was somewhere along the normal ray, the axial movement would be dominant and radial movement would be small. Since the measured data did not reveal a significant radial movement, it suggests that the effective pivot point was closer to the normal ray than to the sliding stage. A family of models can be obtained based on the choice of the pivot point along the normal ray. The choice of a pivot at the pinhole allows for a simpler derivation without loss of generality.

The undesirable rocking motion of the detector can be approximately characterized as a small oscillation of the tilt angle $\Delta\phi$ at the pinhole. Let (u,v) define the coordinate system of the detector. The projection shift Δv caused by the rocking motion can be approximated using the partial derivatives of the simple pinhole projection model, $v=fz/d$, where f is the focal length and d is the distance from AOR to the pinhole (Fig. 6). The postulated rocking of the whole detector at the location of the pinhole will alter the parameter values for d and the origin of the z -axis z^0 .

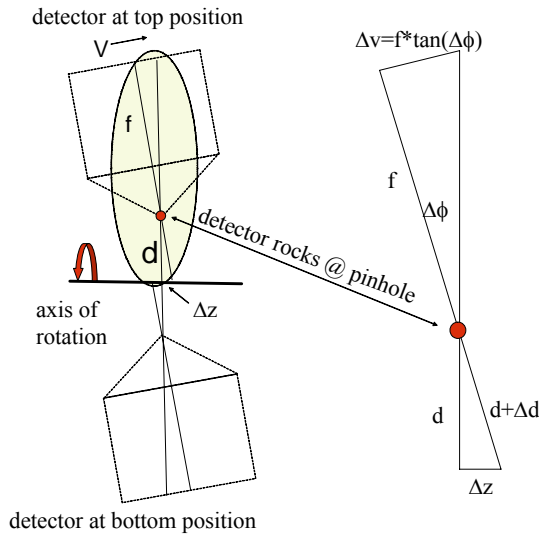


Fig. 6. Figure showing a rocking detector as it rotates from top to bottom position. The normal ray through the pinhole is not stationary at an axial position. The shaded area is shown expanded on right side.

The projection shift Δv can be approximately expressed as:

$$\Delta v = \frac{f}{d}(\Delta z - \frac{z}{d}\Delta d) \quad (1)$$

$$\text{where } \Delta z = d * \tan(\Delta\phi) \approx d\Delta\phi$$

$$\Delta d = d(1/\cos(\Delta\phi) - 1) \approx \frac{1}{2}d(\Delta\phi)^2$$

where Δz and Δd are functions of the tangent and cosine of the rocking angle $\Delta\phi$ respectively. At small tilt angles near zero, it is shown in equation (1) that Δz and Δd have respectively a first and second order effect on Δv . At the focal region where z/d is less than 1, the first term involving Δz is a more significant term. Therefore, we propose a simple model for gantry motion correction, where the correction term is an oscillatory expression due to the Δz component only.

$$\Delta v \approx \frac{f}{d}(d * \tan(\Delta\phi)) = f * \tan(\Delta\phi) \quad (2)$$

Over a complete revolution, the loci of the pinhole describes a circle in a plane that is inclined at a small angle ($\Delta\phi$) to the normal of a rotation axis. The amplitude Δz of axial oscillatory motion is given by $d * \tan(\Delta\phi)$. The parameter Δz is an additional parameter that needs to be fitted. The instantaneous axial displacement g is given by $g = \Delta z * \sin(\theta + \xi)$ where θ is a known detector rotation angle. Besides Δz , the initial detector angular position ξ is another parameter that requires fitting. Similar expressions can be derived for the case of parallel hole collimators.

IV. EXTENSION TO BEQUÉ'S CALIBRATION MODEL

The axial motion term g is along the z direction. It is augmented to the z -coordinate before the 3-orthonormal correctional transformations as described by equation (3). The series of rotational transformations align the coordinate system of the source with that of the detector. The angles (θ, ϕ, ψ) are rotations about the z -, x - and y - axes, respectively.

$$\begin{bmatrix} x''' \\ y''' \\ z''' \end{bmatrix} = \begin{bmatrix} \cos\psi & 0 & -\sin\psi \\ 0 & 1 & 0 \\ \sin\psi & 0 & \cos\psi \end{bmatrix} \begin{bmatrix} 1 & 0 & 0 \\ 0 & \cos\phi & \sin\phi \\ 0 & -\sin\phi & \cos\phi \end{bmatrix} \begin{bmatrix} \cos\theta & 0 & 0 \\ -\sin\theta & \cos\theta & 0 \\ 0 & 0 & 1 \end{bmatrix} \begin{bmatrix} x \\ y \\ z + g \end{bmatrix} \quad (3)$$

After the 3-transformations, the resultant additional terms due to g are:

$$g_{x'''} = -g \cos\phi \sin\psi, \quad g_{y'''} = g \sin\phi, \quad g_{z'''} = g \cos\phi \cos\psi \quad (4)$$

Since ϕ and ψ are usually small angles, the $g_{z'''}$ is the most significant of three additional terms. The extension to Bequé's geometry calibration model is more apparent when projection equations contain the extra axial motion correction terms, $g_{x'''}$, $g_{y'''}$, $g_{z'''}$.

$$v = \frac{-f(m_v - z_0'' - g_{z''})}{d - y_0'' - g_{y''}} + m_v + e_v \quad (5)$$

$$u = \frac{-f(m_u - x_0'' - g_{x''})}{d - y_0'' - g_{y''}} + m_u + e_u$$

where u and v are coordinates in projection space ; m and e are mechanical and electronic shifts. The triple-primed coordinates (x_0''', y_0''', z_0''') denote the transformations without the axial motion term g , as first described in [3]. It is apparent that

$$x''' = x_0''' + g_{x'''} \quad y''' = y_0''' + g_{y'''} \quad z''' = z_0''' + g_{z'''} \quad (6)$$

V. MODEL TESTING

To test the extended geometry calibration model, a phantom consisting of three point sources was used (Fig. 7). The three point sources were arranged in a triangular configuration in a phantom as described in [4]. Projection data was acquired over 360 degree in step of 2 degrees. The projection centroids of the three point sources were calculated.

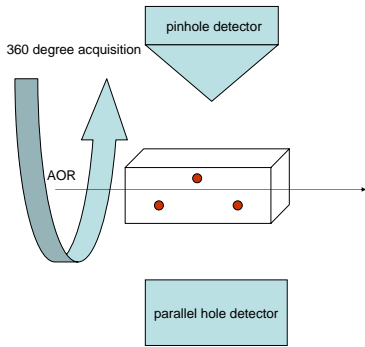


Fig.7. Experimental setup for detector geometry calibration using three point sources in triangular configuration.

The combined objective function F (7) for the pinhole and parallel hole detectors was minimized with respect to a total of twenty two parameters shown in Table 1.

$$F = \sum_i \sum_j \sum_k [(u_{ijk}^{\text{measured}} - u_{ijk}^{\text{predicted}})^2 + (v_{ijk}^{\text{measured}} - v_{ijk}^{\text{predicted}})^2] \quad (7)$$

i : detector index; j : point source index; k : projection index

The pinhole detector contributed nine of the twenty two fitted parameters, while the parallel detector contributed seven. The remaining six fitted parameters were those of the phantom position, whose initially given position were also updated during the optimizing procedure. The combined objective function was minimized using the downhill simplex method available in the IDL.

Table I. Geometry calibration model parameters that are fitted simultaneously.

Model parameters	Pinhole detector	Parallel hole detector
Focal length (f)	yes	n/a
Pinhole-AOR distance (d)	yes	n/a
Tilt angle (ϕ)	yes	yes
Twist (ψ)	yes	yes
Initial detector angular position (θ)	yes	yes
Mechanical shift (m)	yes	yes
Electronic shift (e_u and e_v)	yes	yes
Axial oscillation amplitude (Δz)	yes	yes
Axial oscillation phase (ξ)	yes	yes
Phantom position x		Yes
Phantom position y		Yes
Phantom position z		Yes
Phantom rotation about x		Yes
Phantom rotation about y		Yes
Phantom rotation about z		Yes

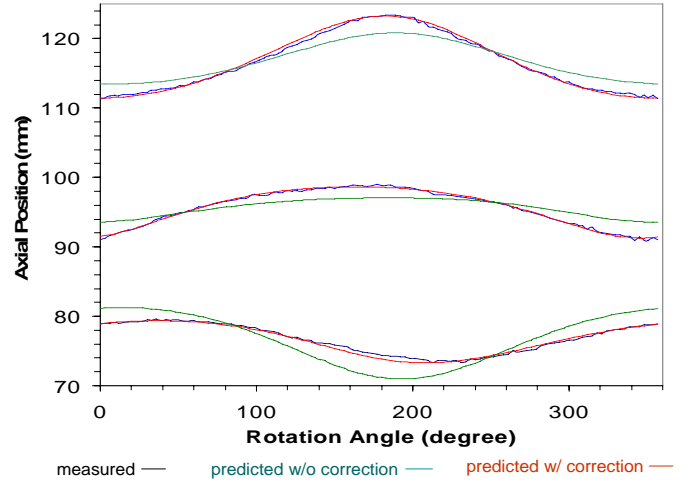


Fig.8. For the pinhole detector, the plots show the measured centroid in axial direction (black) for the three point sources were being closely tracked when axial motion correction was applied (red). Without axial motion correction, tracking was not as accurate (green).

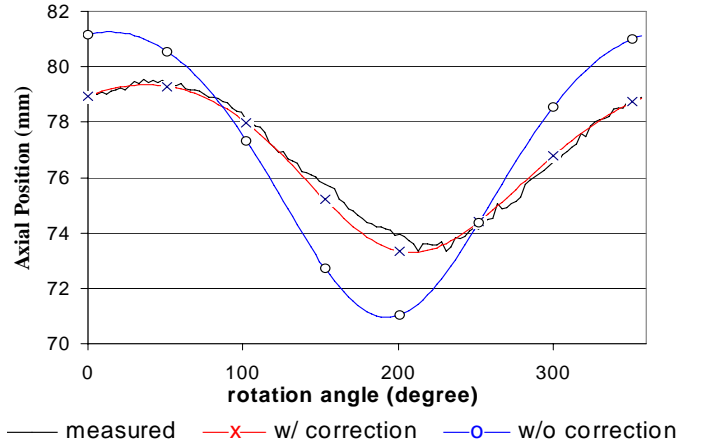


Fig.9. The scaled-up set of 3 plots at bottom part of Fig. 8. For the pinhole detector, the plots show the measured centroid in axial direction (black) were being closely tracked when axial motion correction was applied (red). Without axial motion correction, tracking was not as accurate (blue).

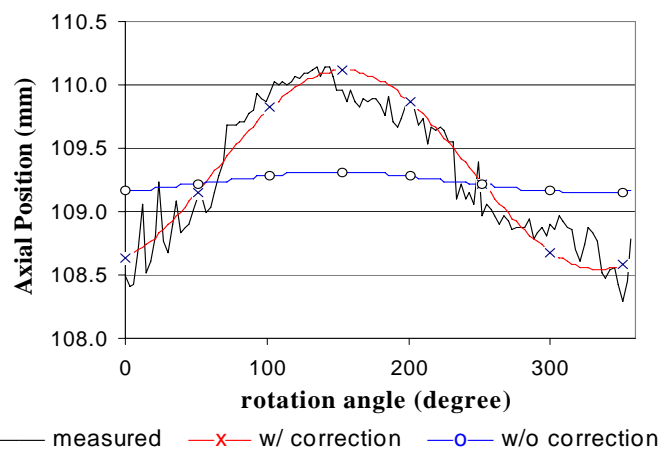


Fig.10. Plots for only one of three point sources for the case of parallel hole detector. The plots show the measured centroid in axial direction (black) were being closely tracked when axial motion correction was applied (red). Without axial motion correction, tracking was not as accurate (blue).

VI. RESULTS

The effectiveness of the proposed axial correction function for geometry calibration is shown in Fig. 8. Predictions in the axial direction closely tracked the measured centroids of the three point sources. Fig. 9 shows the scaled-up plots for one of the three point sources, corresponding to the bottom set of plots shown in Fig. 8. For the parallel hole detector, although the effect due to axial motion is comparatively small, but correction is important for achieving sub-millimeter spatial resolution in small animal imaging applications.

VII. CONCLUSION

We have illustrated the problem of gantry flexing in a gamma ray imaging system with heavy rotating detector heads. We have adapted Bequé's geometry calibration model for a dual-headed SPECT system and introduced additional geometry parameters to account for the observed sinusoidal axial motion. We have shown that with the extended calibration model, the paths of the projection centroids of the three calibration point sources were predicted with improved accuracy.

REFERENCES

- [1] [1] A. G. Weisenberger, et al "Development and testing of a restraint free small animal SPECT imaging system with infrared based motion tracking," NSS Conference Record, IEEE, 2003.
- [2] [2] J. S. Goddard, et al "Real-time landmark-based unrestrained animal tracking system for motion-corrected PET/SPECT imaging," NSS Conference Record, 2002 IEEE, 2002.
- [3] [3] D. Beque, et al "Characterization of pinhole SPECT acquisition geometry," Medical Imaging, IEEE Transactions on, vol. 22, pp. 599-612, 2003.
- [4] [4] D. Beque, et al "Optimization of Geometry Calibration in pinhole SPECT" Medical Imaging, IEEE Transactions on, vol. 24, No. 2, pp. 180-190, 2005.